Optimal wing twist distribution for roll control of MAVs

M. R. Ahmed,
mostafa_aero@yahoo.com
M. M. Abdelrahman
dr_madbouli@hotmail.com
G. M. ElBayoumi
gelbayoumi@yahoo.com
Aerospace Engineering Department
Cairo University
Giza, Egypt

M. M. ElNomrossy
elnomrossy@gmail.com
Production, Energy and Automatic Control Department
French University
Cairo, Egypt

ABSTRACT

The aerodynamic design optimisation of a Micro Air Vehicle (MAV) wing is performed to obtain the optimal anti-symmetric wing twist distribution for the roll control of the MAV's wing instead of using conventional ailerons. This twist distribution should produce minimum induced drag and achieve a better roll response. The implementation of several anti-symmetric load distributions such as the half lemniscates and the Horten distributions is studied leading to an initial solution for the optimal distribution that could achieve better roll requirements. Multhopp's method based on Prandtl's classical lifting line theory is used for the determination of the spanwise load distribution required during the optimisation process. The optimisation process is based on the modified feasible directions gradient based optimisation algorithm implemented in the optimisation system, VisualDOC, given by Dr. Garret Vanderplaats. The proposed optimisation process is applied to the 'BARQ'developed MAV which has successful flight in July 2009.

NOMENCLATURE

a_o	aerofoil lift curve slope (rad^{-1})
AR	aspect ratio
b	span (m)
c	local chord (m)
c_l	local lift coefficient
c_r	root chord (m)
c_t	tip chord (m)
C_L	lift coefficient
C_D	drag coefficient
C_{Di}	induced drag coefficient
C_R	rolling moment coefficient
C_{Yi}	induced yawing moment coefficient
D_i	induced drag force (N)
E	air vehicle's endurance (sec.)
i	incidence angle (radians)
I_x	mass moment of inertia about x-axis (Kg.m^2)
L	lift force (N)
m	number of wing stations solved
M_x	moment about x-axis (N.m)
n	vortex location
q	dynamic pressure (Pa)
Q	amount of electric charge stored in battery
R	air vehicle's range (m)

Paper No. 3647. Manuscript received 10 November 2010, revised version received 13 March 2011, accepted 2 June 2011.

https://doi.org/10.1017/S0001924000006333 Published online by Cambridge University Press

s semi-span (m)
S planform area (m^2)
t_{roll} rolling time (sec.)
TR taper ratio
U free stream velocity (ms^{-1})
V battery's voltage
w_i induced downwash velocity (ms^{-1})
W air vehicle's weight (N)
y wing spanwise station at which the downwash velocity is desired
$\hat{y}$ location of the vortices causing the downwash
α wing geometric angle-of-attack (radians)
$\alpha_{anti\text{-}symmetric}$ anti-symmetric washout distribution (radians)
α_e wing effective angle-of-attack (radians)
α_i wing induced angle-of-attack (radians)
ε downwash angle (radians)
ε_x rolling acceleration (rad/sec^2)
ε_o zero angle-of-attack downwash angle (radians)
γ non-dimensional spanwise circulation strength distribution
Γ spanwise circulation strength distribution
η installed propeller efficiency
λ wing local aspect ratio
ν particular span station where the downwash is to be found
ρ air density (Kg/m^3)
ω_x rolling velocity (rad/sec)
ζ spanwise station where vortices are located

Subscripts

a anti-symmetrical
ht horizontal tail
max maximum
MAV Micro Air Vehicle
s symmetrical
w wing

Superscripts

′ spatial derivative

1.0 INTRODUCTION

Wing morphing is regarded as a promising and efficient mean to achieve better agility and control authority for air vehicles. Many morphing concepts dealing with different aspects of flight control have been introduced recently; however, each is very different in the required shape changes. They involve primarily, small and continuous adjustments in the wing shape[1-3] and/or the surrounding flow field[4] to maneuver the air vehicle during flight. Fortunately, these fast changes for flight control are required in small amplitudes which means that there is never a single solution for a morphing wing, and the technology employed will be vastly different depending on the application required[5]. MAVs are considered an ideal platform for the morphing demonstration as they require quite small power, whereas the benefit is quite large. Besides, the ability to use flexible structures, yet strong enough to support the wing loading, in MAVs rather than larger air vehicles[6,7]. However, the flexible structure required for a morphing wing to generate its new shape in turn would generate aeroelastic forces. These forces would change the shape of the wings influencing the aerodynamic forces.

The use of a morphing wing concept for roll control instead of using conventional ailerons emerged as an important issue for MAVs control. For a MAV to fly efficiently in an urban environment, it should be very agile. Morphing for roll control appears as a promising way in providing efficient control surfaces that would improve this agility and maintain smooth flight[8].

This paper presents a newly developed process for the design of the anti-symmetric twist distribution that should be imposed for the roll control of a MAV wing instead of using conventional ailerons. Only, the aerodynamic design of such morphing wing is presented. The aerodynamic design is performed on two steps. Firstly, the wing geometric characteristics should be obtained through the determination of the wing profile characteristics as thickness and camber distributions (either by designing the appropriate aerofoil or choosing the most suitable one). Besides, the determination of the planform shape of the wing, by identifying the geometric parameters as span, aspect ratio, taper ratio, etc. This wing profile and planform geometric characteristics are determined through the combined optimisation of aerodynamic lift and drag to obtain the symmetric load distribution satisfying the MAV mission and attaining the best stall characteristics for the wing. Secondly, the optimal wing anti-symmetrical twist distribution for initiating a turn is obtained. This distribution should enhance the roll response criteria of the MAV and minimise the induced drag accompanied by this deflection which changes the lift distribution over the wing, hence inevitably increases the induced drag.

The above follows the first and the extended third problems of the 'Three Basic Problems of Wing Theory' formulated for one separate wing by Prandtl. The first problem is called the direct problem in which the lift distribution of the wing is given and wanted is the wing shape (plan form and washout) and its induced drag. While, the



Figure 1. Initial MAV configuration.

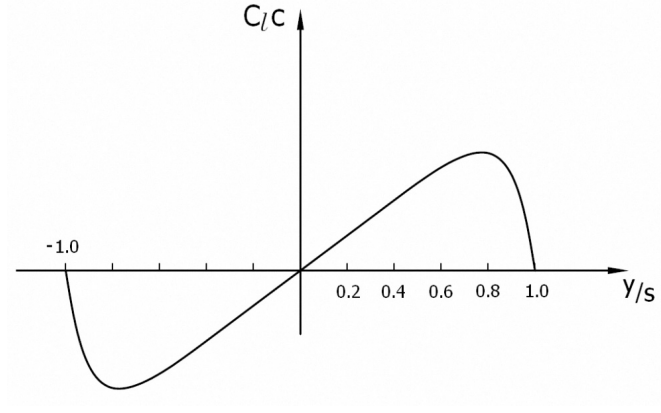


Figure 2. Lift distribution with minimum induced drag for given rolling moment in the form of half lemniscates.

https://doi.org/10.1017/S0001924000006333 Published online by Cambridge University Press

extended third problem is called the optimisation problem in which the overall lift and the rolling moment of a wing together with the induced yawing moment are given and wanted is the lift distribution which has minimum induced drag[9]. Multhopp's method based on Prandtl lifting line theory for the determination of the wing aerodynamic characteristics is used to formulate the optimisation problem. It is used due to its clarity in spite of the fact that it can be applied to flat unswept wings.

The developed optimisation problem is applied to the 'BARQ' MAV for reconnaissance in near field areas. It is designed with elliptic wing as shown in Fig. 1 and having the following mission specifications[10]:

1. Type: Conventional wing-tail arrangement with a maximum dimension not exceeding 40cm.
2. MAV Performance:

Range	up to 1km
Endurance	up to 30min
Flight altitude	about 50m
Cruise speed range	up to 70km/hr
Control	Manual flight mode through a ground operator
Launch status	Hand Launch

3. Payload: The MAV should carry a micro CCD color zoom camera.
4. Data link: The MAV system should process a data link capable of up and down link for both controls; the air vehicle and control as well as transfer the imagery in real time over the defined flight envelop (altitude, range and speed) in the required performance.
5. MAV Mobility: The MAV system should be hand held in one brief case including MAV and the mission control system.

2.0 AERODYNAMIC OPTIMISATION OF WING

The main purpose is to design a new wing for the MAV; hence two optimisation procedures are presented. The first one is to optimise the symmetric load distribution satisfying the MAV mission to get the geometric wing planform and aerofoil spline characteristics. The second one is to optimise the anti-symmetrical load distribution satisfying the roll requirements of the MAV to obtain the optimal wing twist distribution that should be imposed on a MAV's wing instead of using conventional ailerons.

2.1 Symmetrical case

The objective of the aerodynamic optimisation of wing for the symmetrical loading case is to enhance the performance characteristics of the air vehicle during steady level flight through quantifying the wing's geometric parameters. Since the main purpose of the desired MAV system is reconnaissance, therefore enhancing the air vehicle's endurance and/or range allows it to fulfill its mission requirements[11-13]. The main aerodynamic parameters responsible for enhancing the air vehicle's performance are obtained from the endurance and range equations derived for electrically driven air vehicles. Which for the case of steady level flight are given by[14]:

$$E = \frac{\eta VQ}{W^{3/2}}\sqrt{\frac{\rho S_w}{2}}\left(\frac{C_L^{3/2}}{C_D}\right)_{MAV} \quad \ldots (1)$$

$$R = \frac{\eta VQ}{W}\left(\frac{C_L}{C_D}\right)_{MAV} \quad \ldots (2)$$

Thus the aerodynamic quantities that should be optimised are:

- $\left(\frac{C_L^{3/2}}{C_D}\right)_{MAV}$ For endurance case.
- $\left(\frac{C_L}{C_D}\right)_{MAV}$ For range case.

The main contributors to the aerodynamic parameters within the optimisation process are the wing lift and induced drag. These are functions of the lift distribution on the wing, which depends on the particular wing being considered. The prediction of the zero-lift and induced drags for the different air vehicle's components, except the wing induced drag, are modeled by class II methods based on USAF Stability and Control Datcom[15,16]. These methods apply to aircraft with essentially straight, tapered wings. However, the wing's aerodynamic characteristics are obtained using Multhopp's method based on Prandtl's lifting line theory.

2.2 Anti-symmetrical case

The symmetrical lift optimisation gives the optimal wing geometric properties for the case of straight flight. Now, what happens during the turns? In what follows only the simple case of initiating the turn is considered. In this paper a morphing wing capable of imposing an anti-symmetrical twist distribution for the roll control is suggested instead of the use of conventional aileron. This anti-symmetrical deflection changes the lift distribution over the wing, and inevitably increases the induced drag. Hence, for a prescribed rolling moment, the optimum anti-symmetrical lift distribution with respect to the induced drag is required. This distribution should have the property that the induced downwash $w_i(y)$ far behind the wing is proportional to the spanwise coordinate y. This is true for a half lemniscates shown in Fig. 2[9].

The half lemniscates anti-symmetrical lift distribution with optimum induced drag and prescribed rolling moment is[9]:

$$C_l(y)c(y)_{w,a} = \frac{32}{\pi AR_w}C_{R,w}\frac{y}{s_w}\sqrt{s_w^2 - y^2} \quad \ldots (3(a))$$

$$C_{R,w} = \frac{M_x}{qS_w s_w} \quad \ldots (3(b))$$

The coefficient of the induced drag of this anti-symmetrical lift distribution is:

$$C_{Di,w,a} = \frac{8C_{R,w}^2}{\pi AR_w} \quad \ldots (4)$$

The anti-symmetrical lift distribution generates an anti-symmetrical distribution of the induced drags that produces a nearly always non-vanishing induced yawing moment, called adverse yawing moment. For the optimum anti-symmetric lift distribution of the lemniscates shape given by Equation (3), there exists an optimum symmetrical lift distribution with vanishing induced yawing moment. It is given in Equation (5) and shown in Fig 3[9].

$$C_l(y)c(y)_{w,s} = \frac{32}{5\pi AR_w}C_{L,w}(2 - 3\frac{y^2}{s_w^2})\sqrt{s_w^2 - y^2} \quad \ldots (5)$$

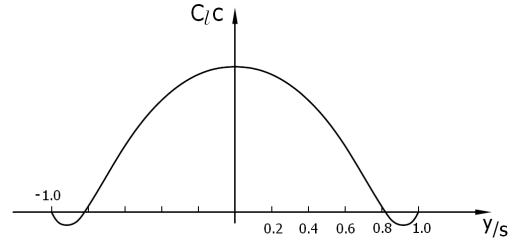


Figure 3. Symmetrical lift distribution which together with the optimum anti-symmetric distribution generates a vanishing induced yawing moment.

https://doi.org/10.1017/S0001924000006333 Published online by Cambridge University Press

The corresponding induced drag which belongs to the Equations (3) and (5) is given by[9]:

$$\pi AR_w C_{Di,w} = 2\cdot 08C_{L,w}^2 + 8C_{R,w}^2 \quad \ldots (6)$$

This means that without a rolling moment, there is a *k*-factor of 2.08. The *k*-factor is the ratio between the coefficient of induced drag of the lift distribution to that of the elliptic lift distribution. The greater the k-factor the worse is the related lift distribution with respect to the induced drag. Hence, this seemingly favorable symmetric lift distribution has an induced drag which exceeds the optimum value of the elliptic lift distribution by 108%. Therefore, this symmetrical distribution although being of a great advantage from the adverse yaw point of view, it produces an extremely large induced drag value making it an unfavorable choice.

Figure 4 shows the Horten symmetrical 'bell-shaped' lift distribution defined by Equation (7) and shown in Fig. 4[9].

$$C_l(y)c(y)_{w,s} = \frac{32}{3\pi AR_w} C_{L,w}\left(1-\frac{y^2}{s_w^2}\right)\sqrt{s_w^2 - y^2} \quad \ldots (7)$$

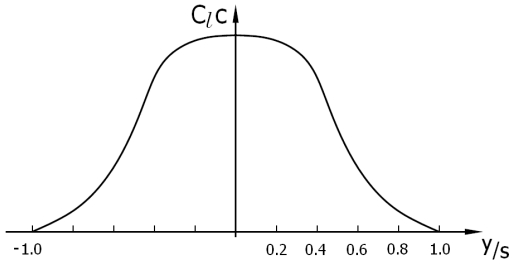


Figure 4. The Horten symmetrical 'bell-shaped' lift distribution.

The anti-symmetric lift distribution corresponding to this symmetric lift distribution with vanishing induced yawing moment is given by Equation (8) and shown in Fig. 5[9].

$$C_l(y)c(y)_{w,a} = \frac{32}{7\pi AR_w} C_{R,w}\left(16\frac{y^2}{s_w^2}-1\right)\frac{y}{s_w}\sqrt{s_w^2 - y^2} \quad \ldots (8)$$

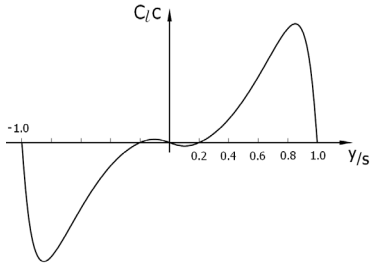


Figure 5. Optimum anti-symmetric lift distribution with vanishing induced yawing moment corresponding to the Horten symmetrical 'bell-shaped' lift distribution.

The corresponding induced drag is given by[9]:

$$\pi AR_w C_{Di,w} = \frac{4}{3}C_{L,w}^2 + \frac{648}{49}C_{R,w}^2 \quad \ldots (9)$$

There is a *k*-factor of 1·33 without rolling moment, which is a quite high 33% loss. Also the additional induced drag due to the anti-symmetric distribution exceeds the values given by Equation (4) by a factor of 1·65. However, the anti-symmetrical Horten distribution is advantageous over the half lemniscates distribution due to its better and faster roll response characteristics. This fact is numerically validated for the current micro air vehicle candidate in the coming sections.

2.3 Spanwise load distribution using Multhopp's spanwise load distribution theory

A method for the definition of the wing aerodynamic characteristics illustrated in the previous sections is required. These characteristics include the determination of the load distributions and their aerodynamic coefficients. They, also, include the twist distribution required for each anti-symmetric load shape. Besides, using this method in defining the required aerodynamic characteristics of the new load distributions generated during the optimisation processes. In this section; Multhopp's method based on Prandtl's lifting line theory is introduced as such method.

The equation for the determination of the spanwise load distribution of a given wing of finite span was first published by Prandtl in 1918[17-23]. The reduced lift at a cross section *y* of a finite span wing is compared with the lift at the same cross section of an infinitely long wing. This reduced lift is due to the change of the incident flow direction that results from the downwash velocity induced by the free vortices. Hence, a profile cross section of a wing of finite span behaves like that of a wing of infinite span (plane flow) at an angle of incidence α_e. The geometric angle-of-attack $\alpha(y)$, measured from the zero-lift position, the effective angle $\alpha_e(y)$, and the induced angle $\alpha_i(y)$ shown in Fig. 6 are related by[17-21]:

$$\alpha(y) = \alpha_e(y) + \alpha_i(y) \quad \ldots (10)$$

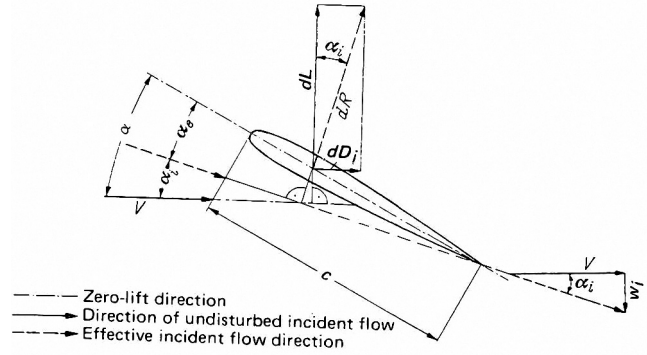


Figure 6. Incident flow directions and evolution of the induced drag[17].

The effective angle-of-attack, $\alpha_e(y)$, is obtained with the help of the Kutta-Joukowsky theorem. While the induced angle-of-attack, $\alpha_i(y)$, is obtained from $\alpha_i(y) = w_i(y)/U$, where, w_i is the distribution of the induced downwash velocity along the span. It is obtained by applying the Biot-Savart law to the semi infinitely long free vortex behind the wing and integrating over the area of the free vortices[17-21].

$$\alpha_e = \frac{2\Gamma(y)}{Uc(y)a_{o,w}} \quad \ldots (11)$$

$$\alpha_i(y) = \frac{1}{4\pi U}\int_{-b_w/2}^{b_w/2} \frac{d\Gamma}{d\hat{y}}\frac{d\hat{y}}{y-\hat{y}} \quad \ldots (12)$$

Introducing Equations (11) and (12) into Equation (10) yields the determination of the circulation distribution. It is a linear integral equation for the circulation distribution $\Gamma(y)$, where Γ depends linearly on the angle-of-attack α.

Solution to the problem of determining the spanwise lift distribution for wings has been presented by Multhopp[17,18]. Starting with the Prandtl's downwash equation; he put a new setup to cover the situation

https://doi.org/10.1017/S0001924000006333 Published online by Cambridge University Press

when y is a variable. Multhopp also assumes that the wing may be replaced by a line vortex and writes the downwash equation as[18]:

$$w(y) = \frac{1}{4\pi}\int_{-b_w/2}^{b_w/2} \frac{d\Gamma}{d\zeta}\frac{d\zeta}{y-\zeta} \quad \ldots (13)$$

The induced angle at y written in a non-dimensional way is then[18]:

$$\alpha_i(\bar{y}) = \frac{1}{2\pi}\int_{-1}^{1} \frac{\gamma'(\bar{\zeta})}{\bar{y}-\bar{\zeta}} d\bar{\zeta} \quad \ldots (14)$$

Where,

$$\bar{y} = \frac{y}{s_w} \qquad \bar{\zeta} = \frac{\zeta}{s_w} \qquad \gamma(\zeta) = \frac{\Gamma(\zeta)}{b_w U}$$

$$d\bar{\zeta} = \frac{d\zeta}{s_w} \qquad \Gamma'(\bar{\zeta}) = s_w\Gamma'(\zeta) \qquad \gamma'(\bar{\zeta}) = s_w\frac{\Gamma'(\bar{\zeta})}{b_w U}$$

While the effective angle at y in a non-dimensional way is[18]:

$$\alpha_e(\bar{y}) = \frac{2\lambda_w}{a_{o,w}}\gamma(\bar{y}) \quad \ldots (15)$$

Introducing Equations (14) and (15) into Equation (10) yields the determination of the non-dimensional circulation distribution through which the local lift coefficient is given by[18]:

$$C_{l,w} = 2\lambda_w\gamma \quad \ldots (16)$$

Turning to the method of finding the local nondimensional circulation γ, the local circulation is a function of the local chord, which of course depends on the particular wing being considered, and the local lift coefficient. The latter is a function of the local lift curve slope which again depends on the particular wing being considered and the local effective angle. The local effective angle is a function of the local induced angle α_i. The local induced angle in Equation (14) is a function of both the vortex locations and the locations of the particular points which combine to give the distance from the vortex to the point. Multhopp's approach at this point is to find the local circulation at several preselected points instead of a completely general solution. A simple method to determine a satisfactory spanwise distribution of arbitrary points where more points near the tips, where the curve changes most rapidly are required, is given according to the relation[17,18]:

$$\theta_v = v\frac{\pi}{m+1} \quad \ldots (17)$$

The span station is then:

$$\bar{\zeta}_v = \mathrm{Cos}(\theta_v) \quad \ldots (18)$$

The local effective angle-of-attack at station v is equal to the local geometric angle-of-attack plus the effect of all the shed vortices[17,18].

$$\alpha_{ev} = \alpha_v + \sum_{n=1}^{m}\Delta\alpha_n \quad \ldots (19)$$

Equation (19) can be written as[17,18]:

$$\alpha_{ev} = b_v\gamma_v = \alpha_v + \sum_{1}^{m} b_{vn}\gamma_n \quad \ldots (20)$$

where b_{vn} is a Multhopp coefficient accounting for the increment of induced angle at station v due to vortex at station, while b_v is a Multhopp coefficient that accounts for the effect of the circulation at station v on that at station n and is equal to $[2\,\lambda_v/a_o\,(v)] + b_{vv}$. In Multhopp's actual solution to obtain the values for the coefficients it develops that[17,18]:

$$b_{vv} = \frac{m+1}{4\mathrm{Sin}(\theta_v)} \quad \ldots (21)$$

$$b_{vn} = \frac{\mathrm{Sin}(\theta_n)}{(\mathrm{Cos}(\theta_v)-\mathrm{Cos}(\theta_n))^2}\frac{1-(-1)^{v-n}}{2(m+1)} \quad \ldots (22)$$

From which both b_{vv} and b_{vn} are always positive and $b_{vn} = 0$ when n-v is an even number. Equation (20) can now be solved for local non-dimensional circulation γ, hence, the local lift coefficient becomes known through Equation (16) and the equation for the total wing lift is[17,18]:

$$L_w = \int_{-1}^{1} qcc_l(\bar{y})d\bar{y} \quad \ldots (23)$$

$$C_{L,w} = AR_w\int_{-1}^{1}\gamma(\bar{\zeta})d\bar{\zeta} \quad \ldots (24)$$

The induced drag is[17,18]:

$$D_{i,w} = \int_{-b_w/2}^{b_w/2}\frac{w}{U}dL \quad \ldots (25)$$

$$C_{Di,w} = AR_w\int_{-1}^{1}\gamma(\bar{\zeta})\alpha_i d\bar{\zeta} \quad \ldots (26)$$

The rolling and the induced yawing moments are[17,18]:

$$C_{R,w} = AR_w\int_{-1}^{1}\gamma(\bar{\zeta})\bar{\zeta}d\bar{\zeta} \quad \ldots (27)$$

$$C_{Yi,w} = AR_w\int_{-1}^{1}\gamma(\bar{\zeta})\bar{\zeta}\alpha_i d\bar{\zeta} \quad \ldots (28)$$

Although being a very weak source of lift compared to the wing, the other secondary source of lift, accounted for, is that produced by the horizontal tail. Its lift is added to that produced by the wing to obtain the total MAV lift during the optimisation process. It could be evaluated from [14,16]:

$$C_{L,ht} = a_{o,ht}\frac{S_{ht}}{S_w}(\alpha(1-(\frac{\partial\varepsilon}{\partial\alpha}))-\varepsilon_o+i_{ht}) \quad \ldots (29(a))$$

$$\alpha = \alpha_w - i_w \quad \ldots (29(b))$$

3.0 APPLICATION OF THE OPTIMISATION PROCESS TO THE 'WING OF MAV'

3.1 Symmetrical case

Since the flight regimes of the MAV wing are at very low subsonic speeds, therefore there is no need for a swept wing. A straight planform wing configuration is chosen; hence only three design variables could serve in completely describing the wing's planform shape. These three variables are chosen to be

1. Wing Span : b_w
2. Wing Aspect Ratio : AR_w
3. Wing Taper Ratio : TR_w

Beside the low subsonic flight regime, the miniature dimensions of the MAV yield to the choice of low Reynold's number aerofoils to be used during the optimisation process. The wing's profile (aerofoil) is allowed to be chosen from the set of low Reynold's

https://doi.org/10.1017/S0001924000006333 Published online by Cambridge University Press

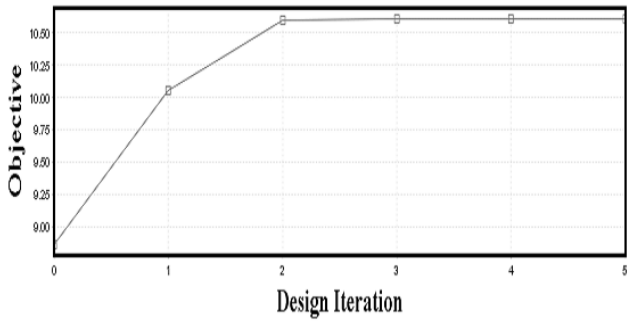


Figure 7. Objective function history during endurance optimisation.

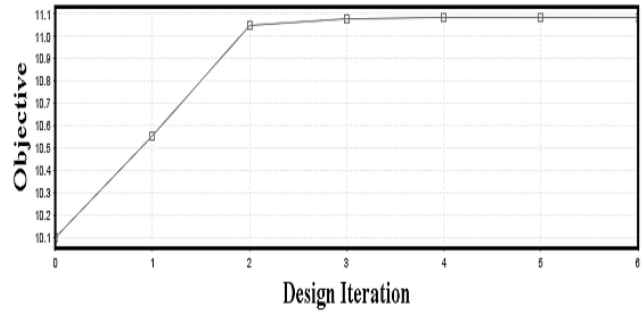


Figure 8. Objective function history during range optimisation.

number aerofoil elaborated by Richard Eppler[24] (E64, E66, E211 and E212). During the optimisation process, the wing span has an upper bound value of 40cm to avoid violation with the mission specifications of the MAV. The wing aspect ratio has a lower bound of four to be in accordance with the assumptions of the lifting line theory. The wing taper ratio is allowed to change between the values 0·4 till a unity value.

The first optimisation problem is formulated so as to enhance the performance of the MAV. The optimisation process is implemented twice; one for maximizing the endurance performance through maximizing the ratio ($C_L^{3/2}/C_D$). The other is for maximizing the range performance through maximizing the ratio (C_L/C_D).The values of the design variables, describing the geometric wing planform and aerofoil characteristics are obtained for both optimisation processes under the constraint of avoiding wing stall; to have a design point away enough from the stall limits. Ensuring a smooth and safe flight is also an important consideration for MAVs flight. Hence, the wing's maximum lift is constrained to be at least greater than the maximum lift the MAV requires by 10%. These conditions are very important in deriving the objectives towards the obtained optimal values, hence, determining the optimal symmetric load distribution satisfying the MAV requirements. The stall problem is the main disadvantage of the initially designed elliptic wing shown in Fig. 1 that leads to choose a tapered configuration instead. Although the elliptic wing configuration has minimum induced drag values, if the wing approaches stall all wing spanwise stations start stalling at the same time which is a very dangerous drawback.

Based on the 'Modified Feasible Directions Gradient Based Algorithm', the optimisation process is implemented in the general purpose optimisation system, VisualDOC[25]. The modified method of feasible directions is a nonlinear optimisation algorithm that combines the features of the method of feasible directions and the generalised reduced gradient method. The algorithm uses the direction-finding subproblem from the method of feasible directions to find a search direction that is equivalent to that of the generalised reduced gradient method. This is without the need of the large number of slack variables associated with inequality constraints. The method of feasible directions has the features that it progresses rapidly to a near optimum design. It requires only gradient information for the objective and active constraints at a given point in the optimisation process. The method has the disadvantages that it is prone to 'zig-zag' between constraint boundaries. It also usually does not achieve a precise optimum. The generalised reduced gradient method is an extension of the reduced gradient method for equality constraints in order to deal with inequality constraints. This method usually converges rapidly to a precise optimum but with a large number of slack variables added to convert inequality constraints to equivalent equality constraints. The modified method of feasible directions used in VisualDOC incorporates the best features of both methods. It is designed specifically for inequality constrained problems. It does not increase the dimensionality of the design problem by adding slack variables to the inequality constraints. It requires only the gradients of the active constraints set, thus reducing both computational effort and computer storage. The method repeats the sub-problem of finding a new usable-feasible search direction, followed by continued search until no search direction can be found that will improve the design without violating one or more constraints[25-27].

The aerodynamic problem illustrated previously is solved in which the configuration of the MAV components (fuselage, horisontal and vertical tail) is fixed and their values during the optimisation process are taken as that of the initially designed MAV[10]. The wing configuration is allowed to change according to the optimisation problem mentioned till reaching the optimum wing configuration. The convergence of the optimisation process is shown through the time histories of the objective functions in Figs 7 and 8, while the final design variables and results are given in Table 1.

The obtained results for both endurance and range optimised configurations are very close from each other from the point of view of dimensions and maximum objective values. Therefore, a final configuration is taken by rounding off the basic dimensions obtained from both optimisation processes. This is to simplify the manufacture procedure through having simple and clean dimensions and without losing a lot in the performance objectives. The final wing configuration is also allowed to have a small sweep angle for the geometric improvement of the wing planform shape. The values of the wing design variables, geometric dimensions, constraints and the aerodynamic objectives of both endurance and range optimised configurations as well as the final configuration are presented in Table 1. A CAD model for the final wing mounted on the MAV is presented in Fig. 9.

Table 1
Optimal values of the design variables, geometric dimensions, constraints and objective functions

Parameter	Endurance Optimised Configuration	Range Optimised Configuration	Final Configuration
Aerofoil	E212	E212	E212
Wing span, b_w (cm)	39·9	40	40
Wing aspect ratio, AR_w	5·065	5·054	5
Wing taper ratio, TR_w	0·6275	0·6522	0·6
Wing area, S_w (cm^2)	316	317	320
Wing root chord, $c_{r,w}$ (cm)	9·705	9·582	10
Wing tip chord, $c_{t,w}$ (cm)	6·089	6·249	6
Wing quarter chord Sweep angle (deg.)	–	–	3
$C_{L,w,max}/C_{L,MAV,max}$	1·0997	1·1002	1·1118
$(C_L^{3/2}/C_D)_{MAV}$	10·6361	10·6271	10·53
$(C_L/C_D)_{MAV}$	11·08	11·09	11·02

https://doi.org/10.1017/S0001924000006333 Published online by Cambridge University Press

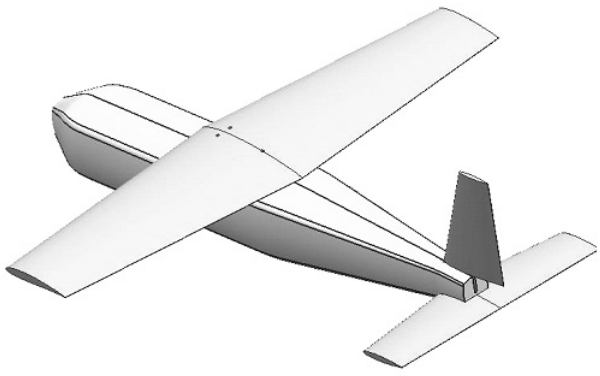


Figure 9. Final wing configuration installed on MAV.

The load distribution is plotted for the final wing candidate for the two flight conditions:

1. Condition #1: condition where the MAV attains a maximum value of $C_L^{3/2}/C_D$.
2. Condition #2: condition where the MAV attains a maximum value of C_L/C_D.

Results are presented in Figs 10 and 11 while the values of the total wing lift and induced drag are given in Table 2.

Table 2
Results of total wing lift and induced drag

Point of comparison	$C_{L,w}$	$C_{Di,w}$
Condition#1	1·0084	0·0657
Condition#2	0·7491	0·0363

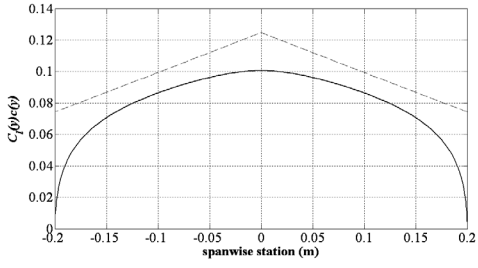


Figure 10. Wing load distribution at condition #1.

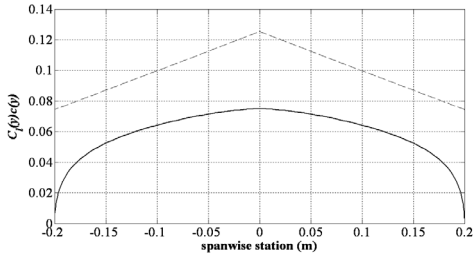


Figure 11. Wing load distribution at condition #2.

3.2 Anti-symmetrical case

Based on the previous discussion, the implementation of several anti-symmetric load distributions such as the half lemniscates and the Horten distributions is studied when added to the obtained optimised symmetric part of the load distribution, which is neither elliptic nor Horten. A comparison is done from point of view of the rolling moment coefficient, C_R, the induced drag coefficient, C_{Di}, the induced yawing moment coefficient, C_{Yi} and the roll response of each distribution. The symmetric load distribution is taken that at condition #2 to be as far as possible from the stall limits during roll maneuver.

In order to obtain the anti-symmetrical load distribution on the wing, the required rolling moment coefficient should be calculated. Using fundamental laws of mechanics and assuming a constant rolling acceleration for the MAV, it could be shown that:

$$M_x = I_x \varepsilon_x \quad \ldots (30)$$

$$C_{R,w} = \frac{2 I_x \omega_x}{t_{roll} q \, S_w s_w} \quad \ldots (31)$$

Since there are no roll qualities specified except for the military standard[28], it is used to choose good values for ω_x and t_{roll} . These are chosen as ω_x = 20deg./sec and t_{roll} = 1sec. According to these values, the required rolling moment coefficient could be calculated. The imposed anti-symmetric washout distribution should produce a rolling moment coefficient which is at least equal to this required rolling moment coefficient. The load change on the wing as well as the required anti-symmetric twist distributions required for roll control for both the half lemniscates and the Horten distributions given by Equations (3) and (8) respectively are shown in Figs from 12 to 15.

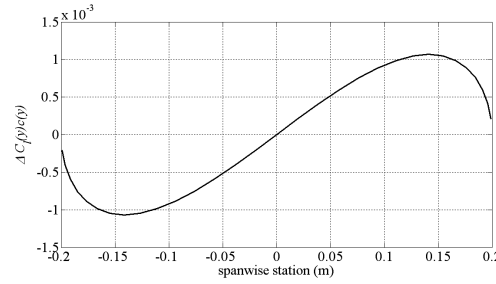


Figure 12. Anti-symmetric load change for the half lemniscates distribution.

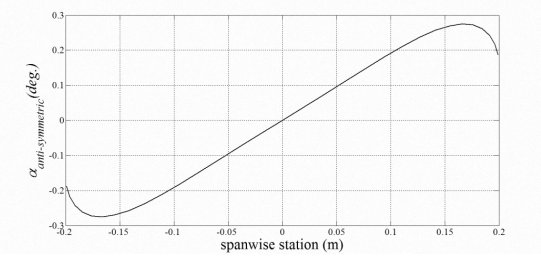


Figure 13. Anti-symmetric twist distribution for the half lemniscates distribution.

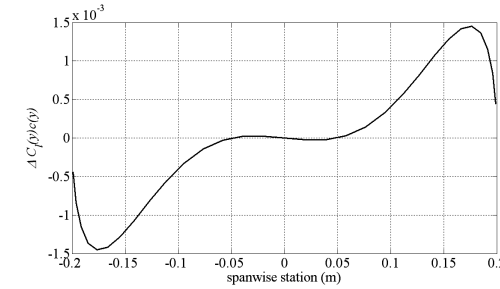


Figure 14. Anti-symmetric load change for the Horten distribution.

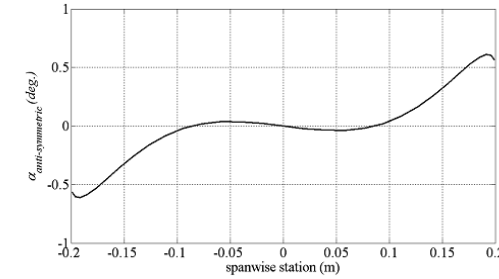


Figure 15. Anti-symmetric twist distribution for the Horten distribution.

https://doi.org/10.1017/S0001924000006333 Published online by Cambridge University Press

As mentioned earlier the optimum anti-symmetric load distribution with respect to the induced drag is that of a half lemniscates. However, the roll response of the anti-symmetric Horten distribution is better. A quantitative way to show this advantage with respect to roll response could be illustrated upon plotting the response of the MAV to step function inputs of the mean morphing angle[29,30]. This is shown in Figs from 16 to 18, where, it becomes clear that the Horten distribution has always a faster roll response attitude than that of the half lemniscates.

An optimisation process is implemented in which the Horten distribution is considered as an initial solution and the objective is minimising the induced drag. Hence, better response characteristics are obtained as well as minimum induced drag. Referring to Fig. 15, the anti-symmetric washout distribution due to the Horten distribution could be approximated by zero distribution from root section till half of the semi span. From the half semi span section till the tip; it could be approximated as third degree polynomial:

$$\alpha_{anti\text{-}symmetric} = ay^3 + by^2 + cy + d \quad \ldots (32)$$

Where, y is the spanwise co-ordinate valid in the range ($0{\cdot}1\text{m} \le y \le 0{\cdot}2\text{m}$). The second optimisation problem is formulated so as to minimise the induced drag due to anti-symmetrical load distribution to find the values of the coefficient a, b, c and d under the constraint that the rolling coefficient produced by the wing is greater than that required for the maneuver of the MAV. This optimisation process is carried once again using the VisualDOC optimisation system based on the modified method of feasible directions. The convergence of the optimisation process is shown through the time history of the objective function in Fig. 19. The values of the coefficients of the optimised anti-symmetrical distribution are: $a = -12{\cdot}8564$, $b = 4{\cdot}8426$, $c = -0{\cdot}4757$ and $d = 0{\cdot}012$. The load change on the wing as well as the required anti-symmetric twist distributions required for roll control for the optimised distribution is shown in Figs 20 and 21. While, the values of the total wing rolling moment coefficient, induced drag coefficient due to the imposed anti-symmetrical distribution as well as the induced yawing moment coefficient are given in Table 3.

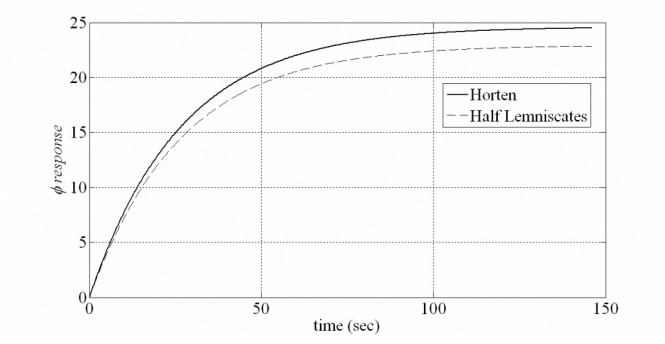


Figure 16. Bank angle response to step function input of morphing mean angle.

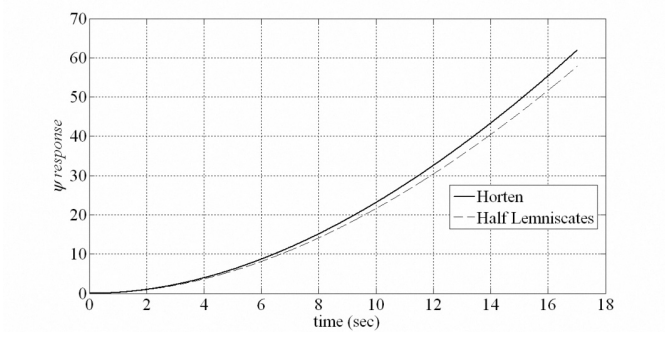


Figure 17. Heading angle response to step function input of morphing mean angle.

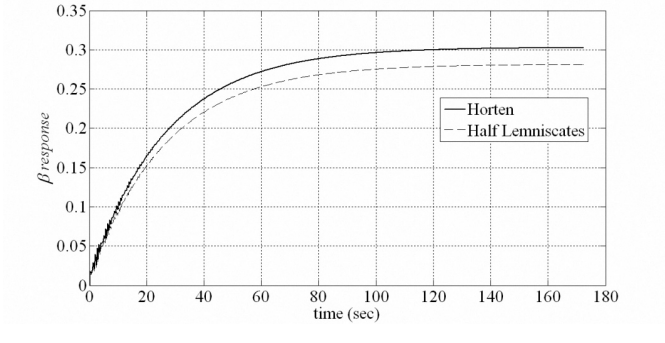


Figure 18. Side slip angle response to step function input of morphing mean angle.



Figure 19. Objective function time history during anti-symmetrical load optimisation.

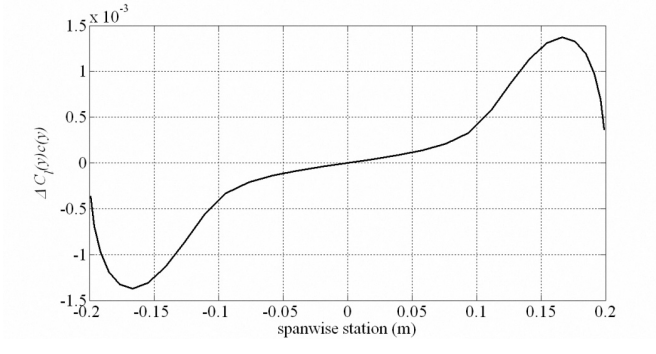


Figure 20. Anti-symmetric load change for the optimum distribution.

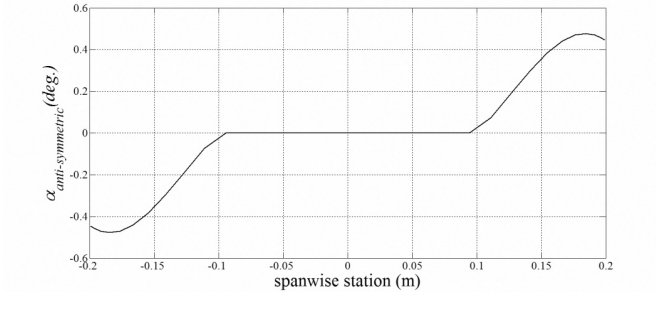


Figure 21. Anti-symmetric twist distribution for the optimum distribution.

https://doi.org/10.1017/S0001924000006333 Published online by Cambridge University Press

Table 3
Comparison between the three anti-symmetrical load distributions from point of view of C_R, C_{Yi} and C_{Di}

Point of comparison	Half lemniscates distribution	Horten distribution	Optimum distribution
$C_{R,w}$	0·0052	0·0052	0·0052
$C_{Yi,w,a}$	8·1509E-4	9·0981E-4	8·7688E-4
$C_{Di,w,a}$	1·3957E-5	2·2984E-5	1·9815E-5
$C_{Di,w,a}$ percentage increase from the half lemniscates distribution	0	65	41

Table 3 shows that for the same rolling moment coefficient, the induced drag produced by the optimised anti-symmetrical twist distribution is less than that produced by the Horten distribution by twenty four percent. However, it could achieve the same roll response as the Horten distribution. Although, it's induced drag is still greater than that produced by the half lemniscates distribution, the optimum twist distribution succeeded to have better roll response characteristics with the induced drag minimised as possible. It is of importance to mention that the above optimisation procedure could be repeated to obtain different anti-symmetrical load distribution shapes and the corresponding twist distributions for different rolling moments. These optimum wing twist distributions could be implemented using an active feedback control system and a morphing mechanism capable of producing a third degree polynomial twist distribution. This is simpler to apply on a MAV rather than a large air vehicle. In this manner optimal twist distribution could be maintained as the rolling requirements change.

4.0 CONCLUSIONS

The proposed aerodynamic optimisation of the twist distribution on a MAV's wing shows that:

- The obtained anti-symmetric twist distribution satisfies the roll requirements of the micro air vehicle as well as providing minimum induced drag and better response characteristics.
- The use of Multhopp's procedure based on Prandtl's lifting line theory can be easily used for such type of wing for this category of air vehicles.
- The modified feasible directions gradient based optimisation algorithm converges rapidly for the solution of wing twist design of MAV.

REFRENCES

1. SANDERS, B., EASTEP, F.E. and FORSTER, E. Aerodynamic and aeroelastic characteristics of wings with conformal control surfaces for morphing aircraft, *AIAA J Aircr*, January-February 2003, **40**, (1), pp 94–99.
2. HALL, J.M. Executive summary AFTI/F-111 mission adaptive wing, WRDC TR-89-2083, September 1989.
3. KHOT, N.S., ZWEBER, J.V., VELEY, D.E., OZ, H. and EASTEP, F.E. Flexible composite wing with internal actuation for roll maneuver, *AIAA J Aircr*, July-August 2002, **39**, (4), pp 521–527.
4. NATARAJAN, A., KAPANIA, R.K. and INMAN, D.J. Aeroelastic optimisation of adaptive bumps for yaw control, *AIAA J Aircr*, January-February 2004, **41**, (1), pp 175–185.
5. BOURDIN, P., GATTO, A. and FRISWELL, M.I. Aircraft control via variable cant-angle winglets, *AIAA J Aircr*, March-April 2008, **45**, (2), pp 414–423.
6. IFJU, P., ETTINGER, S., JENKINS, D. and MARTINEZ, L. Composite materials for micro air vehicles, *SAMPE J*, 2001, **37**, (4), pp 7-13.
7. ABDULRAHIM, M., GARCIA, H. and LIND, R. Flight characteristics of shaping the membrane wing of a micro air vehicle, *AIAA J Aircr*, January-February 2005, **42**, (1), pp 131–137.
8. STANFORD, B., ABDULRAHIM, M., LIND, R. and IFJU, P. Investigation of membrane actuation for roll control of a micro air vehicle, *AIAA J Aircr*, May-June 2007, **44**, (3), pp 741–749.
9. NICKEL, K. and WOHLFAHRT, M. *Tailless Aircraft in Theory and Practice*, American Institute of Aeronautics and Astronautics, Washington DC, USA, 1994.
10. An Independent Internal Report Design and development of a Micro Air Vehicle, Aerospace Engineering Department, Cairo University, Giza, Egypt, 2009.
11. ROSKAM, J. *Airplane Aerodynamics and Performance,* Design, Analysis and Research Corporation, Lawrence, Kansas, USA, 1997.
12. ANDERSON, J.D. *Aircraft Performance and Design*, WCB/McGraw-Hill, International edition, 1999.
13. ANDERSON, J.D. *Introduction to Flight*, McGraw-Hill, New York, USA, 1978.
14. AHMED, M.R., ABDELRAHMAN, M.M., ELNOMROSSY, M.M. and ELBAYOUMI, G.M. Aerodynamic shape optimisation of Micro Air Vehicle wing, Proceedings of 10TH International Congress of Fluid Dynamics, ICFD10-EG-3076, Ain Soukhna, Red Sea, Egypt, 2010.
15. HOAK, D.E. *et al*, USAF Stability and Control Datcom, Flight Control Division, Air Force Flight Dynamics Laboratory, Ohio, USA, 1978.
16. ROSKAM, J. *Airplane Design, Part VI,* Design, Analysis and Research Corporation, Lawrence, Kansas, USA, 1989.
17. SCHILICHTING, H. and TRUCKENBRADT, E. *Aerodynamics of the Airplane*, McGraw-Hill, New York, USA, 1979.
18. POPE, A. *Basic Wing and Aerofoil Theory*, McGraw-Hill, New York, USA, 1951.
19. PRANDTL, L. Applications of modern hydrodynamics to aerodynamics, NACA TR-116, June 1921.
20. BERTIN, J.J. *Aerodynamics for Engineers*, Prentice-Hall, Upper Saddle river, NJ, USA, 2002.
21. ANDERSON, J.D. *Fundamentals of Aerodynamics*, McGraw-Hill, New York, USA, 2001.
22. PHILIPS, W.F. Lifting-Line analysis for twisted wings and wash out optimized wings, *AIAA J Aircr*, January-February 2004, **41**, (1), pp 128- 136.
23. PHILIPS, W.F., ALLEY, N.R. and GOODRICH, W.D. Lifting-line analysis of roll control and variable twist, *AIAA J Aircr*, September-October 2004, **41**, (5), pp 1169-1176.
24. EPPLER, R. *Aerofoil Design and Data*, Springer Verlag, Berlin, Germany, 1990.
25. VisualDoc Version 6.2 Users and Theory Manuals, Vanderplaats Research and Development, 2009.
26. VANDERPLAATS, G.N. *Numerical Optimisation Techniques for Engineering Design*, Vanderplaats Research and Development, 1999.
27. VANDERPLAATS, G.N. An Efficient feasible directions algorithm for design synthesis, *AIAA J*, November 1984, **22**, (11), pp 633-640.
28. Military Specification, Flying Qualities of Piloted Airplanes, MIL-F-378SC, November 1980.
29. ETKIN, B. *Dynamics of Flight, Stability and Control*, John Wiley & Sons, New York, USA, 1963.
30. ROSKAM, J. *Airplane Flight Dynamics and Automatic Flight Control,* Design, Analysis and Research Corporation, Lawrence, Kansas, USA, 2007.

https://doi.org/10.1017/S0001924000006333 Published online by Cambridge University Press